Shear wave velocity and soil type microzonation using Neural Networks and Geographic Information System

Mohammad Motalleb Nejad[1], Mohammad Sadegh Momeni [2], Kalehiwot Nega Manahiloh [3]

Abstract

Frequent casualties and massive infrastructure damages are strong indicators of the need for dynamic site characterization and systematic evaluation of a site's sustainability against hazards. Microzonation is one of the most popular techniques in assessing a site's hazard potential. Improving conventional macrozonation maps and generating detailed microzonation is a crucial step towards preparedness for hazardous events and their mitigation. In most geoscience studies, the direct measurement of parameters imposes a huge cost on projects. On one hand, field tests are expensive, time-consuming, and require specific high-level expertise. Laboratory methods, on the other hand, are faced with difficulties in perfect sampling. These limitations foster the need for the development of new numerical techniques that correlate simple-accessible data with parameters that can be used as inputs for site characterization. In this paper, a microzonation algorithm that combines neural networks (*NNs*) and geographic information system (*GIS*) is developed. In the field, standard penetration and downhole tests are conducted. Atterberg limit test and sieve analysis are performed on soil specimens retrieved during field-testing. The field and laboratory data are used as inputs, in the integrated *NNs-GIS* algorithm, for developing the microzonation of shear wave velocity and soil type of a selected site. The algorithm is equipped with the ability to automatically update the microzonation maps upon addition of new data.

Keywords: Geographic information system (*GIS*); neural networks (*NNs*); shear wave velocity (V_s); in-situ testing; unified soil classification system (*USCS*); microzonation; standard penetration test (*SPT*); Atterberg limits.

Citation information: please cite this work as follows

Motalleb Nejad, M., M.S. Momeni, and K.N. Manahiloh, *Shear wave velocity and soil type microzonation using neural networks and geographic information system.* Soil Dynamics and Earthquake Engineering, 2018. **104**: p. 54-63.

[1] University of Delaware, Civil and Environmental Engineering, 301 DuPont Hall, Newark, DE 19711

[2] ZTI Consulting Engineers, 32 2nd Kousar, Sattarkhan Street. Tehran, Iran

[3] Corresponding Author: University of Delaware, Civil and Environmental Engineering, 301 DuPont Hall, Newark, DE 19711, E-mail: knega@udel.edu, Phone: 302-831-2485, Fax: 302-831-3640

Introduction

Casualties and massive infrastructure destruction are great indicators of the need for systematic characterization of a site's sustainability against natural disasters. Microzonation has been known as one of the most accepted tools in assessing soil failure potentials. Seismic microzonation is a generic name for the process of subdividing a seismic-prone area into zones based on appropriately selected geotechnical properties. This process can be done by systematically estimating the response of soil layers to earthquake excitations. The result of a microzonation process is a geographical map—generated in terms of suitable geotechnical and geophysical parameters—illuminating specific geological characteristics of a site, such as soil type, or the potential of different zones of a site for geotechnical failures, such as ground shaking, liquefaction, landslide, tsunami, and flooding. One example parameter that can be used in microzonation is the small-strain shear modulus (also called maximum shear modulus, G_{max}). G_{max} can be correlated to the deformation potential of a given site against seismic actions. This parameter has been discovered to have a direct correlation with the small-strain shear wave velocity of a soil [1]. In other words, shear wave velocity in low strains can be used as a unique and reliable parameter that can be used in microzonation maps.

Making improvements on the traditional macrozonation maps and generating detailed microzonation maps is a crucial step towards preparedness for future hazardous events. In the last few decades, efforts were made to perform microzonation on different earthquake-prone areas to be used for construction and design purposes. Fäh, Rüttener, Noack and Kruspan [2] carried out a detailed microzonation of the city of Basel to perform a numerical modelling of expected ground motions during earthquake events. Tuladhar, Yamazaki, Warnitchai and Saita [3] performed a seismic microzonation for the city of Bangkok by using micro-tremor

observations. Anbazhagan and Sitharam [4] mapped the average shear wave velocity for the Bangalore region in India. They also proposed an empirical relationship between the Standard Penetration Test blow count (*SPT-N*) and shear wave velocity. Vipin, Sitharam and Anbazhagan [5] carried out a performance-based liquefaction potential analysis based on *SPT* data acquired from Bangalore, India. Cox, Bachhuber, Rathje, Wood, Dulberg, Kottke, Green and Olson [6] presented a seismic site classification microzonation of the city of Port-au-Prince based on shear wave velocity of the soil and provided a code-based classification scheme for the city. Murvosh, Luke and Calderón-Macías [7] carried out shear wave velocity profiling in complex ground to enhance the existing microzonation of Las Vegas. Kalinina and Ammosov [8] studied the applicability of multichannel analysis of surface waves to address the solutions for microzonation problems.

For a good microzonation, it is not only important to obtain reliable data from field measurements but also to identify and implement a robust technique to optimize the input-output relationship. Most of the statistical methods require a significant volume of data to produce reliable results. Direct measurement of most geotechnical parameters imposes huge costs on projects. Field tests are time-consuming and need specific expertise. Laboratory methods, on the other hand, are faced with difficulties from imperfect sampling. These limitations necessitate the development of numerical techniques that correlate easily accessible data with parameters that require extensive effort. In light of this, Artificial Intelligence (*AI*) integrated with *GIS* can be used to model the seismic hazard susceptibility of a site.

Fuzzy Networks, metaheuristic algorithms, and most importantly, neural networks (*NNs*) can all be categorized under the field of *AI*. *NNs* are designed to approximate complicated non-linear correlations between input and output layers of a specific problem while using a small fraction of

data for training purposes [9-11]. Furthermore, *NNs* are designed to eliminate the complicated statistical variables that exist in conventional statistical methods [12]. The integration of *NNs* with *GIS* has recently been tried for various problems [13]. Li and Yeh [14] used this approach to simulate multiple land use changes in southern China. Pijanowski, Brown and Shellito [15] proposed a model to evaluate the land transformation. Lee, Ryu, Min and Won [12] used an integrated *GIS* and *NNs* to study the landslide susceptibility in the area of Yongin in Korea. Pradhan and Lee [16] analyzed the regional landslide hazard utilizing optical remote sensing data. Yoo and Kim [17] predicted the tunneling performance required in routine tunnel design works. Pradhan, Lee and Buchroithner [18] proposed a *GIS*-based neural network model to obtain landslide susceptibility mapping for risk analysis. Ho, Lin and Lo [19] proposed a methodology to assess the water leakage and prioritize the order of pipe replacement in a water distribution network.

In this study, *NNs* have been used to correlate easily obtainable geotechnical parameters with parameters that govern the seismic potential of a soil. The resulting correlation has been implemented in generating microzonation maps. Python coding has been implemented to develop a dynamic system capable of automatically improving microzonation maps as additional data is acquired and inserted. The proposed algorithm has been applied for the microzonation of Urmia City, which is located in the northeastern part of Iran. In the succeeding sections of the paper, the design and implementation of an integrated system that performs geotechnical microzonation of a site will be presented.

Methods and Materials

Neural Networks (NNs)

Neural networks are known to be the main and inspiring branch of artificial intelligence. It is not an overstatement to claim that the word intelligence is an appropriate attribute for neural networks, since the *NNs* algorithms are based on simplified mathematical models for the interconnected electro-chemical transmitting neurons, what we call it "Brain" [20]. *NNs* are designed to extract non-linear correlations between effective variables by examining a large set of responses. Neural networks are primarily trained with a large data set. *NNs* are able to provide accurate output for a data set if a proper training plan has been implemented. Correctly, designed *NNs* will have three main parts: the transfer function, the network structure, and the learning law. These parts are defined separately based on the type of the defined problem [21].

NNs consist of an interaction between several interconnected nodes, called artificial neurons. These neurons exchange messages with each other. These neurons could be located in several different layers. The structure of designed *NNs* includes three different types of layers: (1) input layer (2) hidden layer(s) and (3) output layer. Each structure has one input layer and one output layer. Hidden layers are intermediate layers defined between the input and output layers where the active signals are transmitted between layers. The number of hidden layers and nodes per layer are set based on trial and error by the network's designer. The connections between neurons have numeric weights that can be adjusted based on experience. This feature helps the *NNs* learn from experience. Each weighted neuron connection is activated by a transform function in a given layer. This process is repeated until the output neurons are all activated. The error of the *NNs* is defined as the difference between the *NNs* output and the given observation. The weights are then changed until the error is minimized. The minimization of the error can be performed

with different types of optimization techniques. Metaheuristic methods such as the harmony search algorithm have been used in several engineering problems [22, 23]. Least squares methods can also be used to minimize the error.

From a number of different types of *NNs*, a feedforward network is selected here. Such a network uses backpropagation (*BP*) technique—a gradient descent algorithm in which the network weights are moved along the negative of the gradient of the performance function. In this study, the Levenberg-Marquardt (*LM*) algorithm [24] is employed to optimize the weight of networks. This algorithm has the capability of solving non-linear least squares problems. For the basic *BP* algorithm, the weights of the network are adjusted in the direction that the rate of descent for the performance function is highest. The weight of the network for each iteration is calculated from the following expression:

$$\mathrm{W}_{k+1} = \mathrm{W}_k - \alpha_k \mathrm{G}_k \qquad (1)$$

where W_k is a vector of current weights, $\mathbf{G}_k$ is the current gradient, and α_k is the learning rate. For fast optimization, the gradient can be replaced by the Hessian matrix of the performance index at the current values of the weights $(\mathbf{A}_k^{-1})$. Since a huge computational effort is required to obtain the Hessian matrix for feedforward neural networks, the *LM* algorithm has been designed to approach a second-order training speed without the need to calculate the Hessian matrix [25]. For the performance function with the form of a sum of squares, the Hessian matrix can be approximated by:

$$\mathbf{H} = \mathbf{J}^{\mathrm{T}}\mathbf{J} \qquad (2)$$

$$\mathrm{G} = \mathbf{J}^{\mathrm{T}}\mathrm{E} \qquad (3)$$

where **J** is the Jacobian matrix that contains the first derivatives of the network errors with respect to the weights, and E is a vector of network errors.

The Jacobian matrix can be computed through a standard backpropagation technique [25] which bypasses the difficulty of computing the Hessian matrix. The *LM* algorithm uses this approximation to the Hessian matrix in the following Newton-like update:

$$W_{k+1} = W_k - [\mathbf{J}^T\mathbf{J} + \mu\mathbf{I}]^{-1}\mathbf{J}^T E \quad (4)$$

The correction factor μ is a counterweight that guarantees the reduction of the performance function. Any increase or decrease in performance function is accompanied by mutual increase or decrease in the correction factor. This way, the performance function is always reduced at each iteration of the algorithm [26].

Overfitting is the most common problem that may occur during the training process. This problem occurs when the obtained error for the training set of the data is very small but that of the testing data is very large. The network has memorized the training examples, but it has not learned to generalize to new situations (i.e., testing data). Regulation is a technique that prevents overfitting and improves network generalization. It involves modifying the performance function, which is normally chosen to be the sum of squares of the network errors in the training set.

The performance of a neural network is evaluated by a correlation coefficient (*r*), mean absolute error (*MAE*), and root mean square error (*RMSE*). The correlation coefficient is defined as:

$$r = \frac{\sum_{i=1}^{n}(O_i - \overline{O})(T_i - \overline{T})}{\sqrt{\sum_{i=1}^{n}(O_i - \overline{O})^2}\sqrt{\sum_{i=1}^{n}(T_i - \overline{T})^2}} \quad (5)$$

The mean absolute and root mean square errors are defined as follows:

$$MAE = \frac{\sum_{i=1}^{n} |T_i - O_i|}{n} \quad (6)$$

$$RMSE = \sqrt{\frac{\sum_{i=1}^{n} (T_i - O_i)^2}{n}} \quad (7)$$

where T_i and O_i are the target output and the output calculated by the neural network, respectively.

The performance function used for training neural networks is the root mean sum of squares of the network errors. It is possible to improve generalization if the performance function is modified by adding a term that consists of the root mean of the sum of squares of the network weights as:

$$rmse_{\text{reg}} = \gamma\, rmse + \frac{(1-\gamma)}{\text{n}} \sum_{\text{j}=1}^{\text{n}} W_{\text{j}}^2 \quad (8)$$

where γ and n are the performance ratio and number of network weights, respectively.

This performance function causes the network to have smaller weights and forces the network response to be smoother and less likely to overfit [27].

To model the nonlinear behavior of the communication mechanism in a neuron, an activation function has to be introduced to a layer's net input. Transfer functions calculate a layer's output from its net input [28]. Different forms of nonlinear mathematical models have been suggested and used in various engineering applications. In this study, based on trial and error, the tangent sigmoidal (*Tansig*) transfer function has been employed:

$$a = \tan sig(x) = \frac{2}{1+\exp(-2x)} - 1 \qquad (9)$$

where a is the output of the current layer and input of the next layer, and x is the input of the current layer. The *Tansig* transfer function is shown in Fig. 1.

Integration of GIS with NNs

In this work, a novel dynamic algorithm has been developed to collect data from geographic information systems, and Python® has been employed to link *NNs* to *GIS*. First, the system searches for any deficiency in data over the entire domain of layers. For each layer, if any data is missed, the ordinary kriging method [29] is used to do interpolation, and the spatial information associated with the missed data points are extracted and added to the data set. Then the complete data is used to design *NNs*. *NNs* are trained for the available data based on the optimum number of hidden layer nodes and internal parameters such as momentum term and learning rate. For a given data set, 80% of it is used for training, and the remaining 20% is used for evaluation purposes.

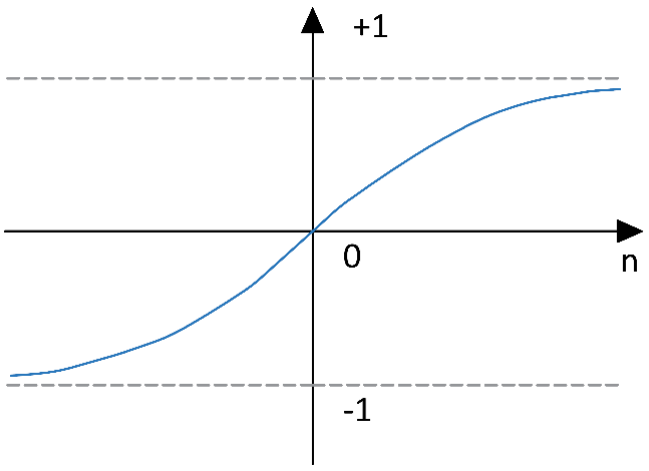

Fig. 1 - Tangent sigmoidal (*Tansig*) transfer function

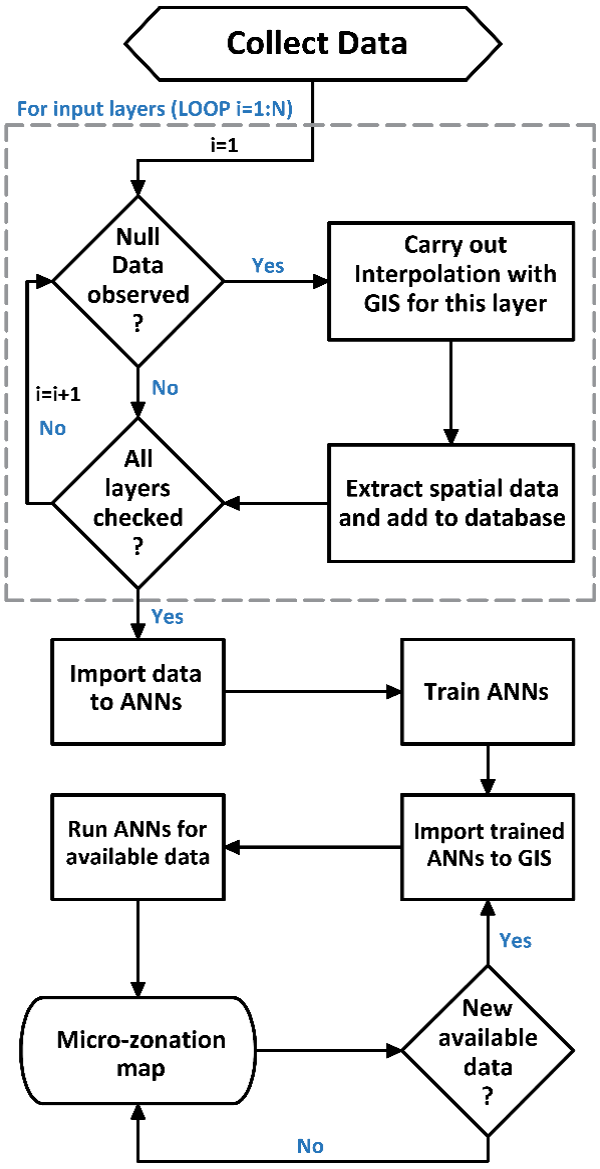

Fig. 2 - Flowchart of the proposed integrated dynamic system.

The trained *NNs* are then embedded in a *GIS* platform using Python scripts to dynamically update microzonation maps. Fig. 2 shows a flowchart of the integrated dynamic system idealized as a three-step process. In step 1, null data lags are filled. Steps 2 and 3 embed the trained *NNs* in *GIS* and update the microzonation map, respectively. Once all layers are covered, steps 1 and 2 freeze, and step 3 dynamically updates the microzonation with new details as newly collected information is added to the database.

Laboratory and Field Experiments

Location of the experimental work

The city of Urmia is located 1330 meters above sea level with geographic coordinates, 37°33’19”N 45°04’21”E. Urmia is the 10th most populated city in Iran (with a population of 667,499 in 2012). The city is the trading center for fruit produce, which is the source of its nickname “the city of apples and grapes”. One of the world’s largest salt lakes, “Lake Urmia”, is located east of the city and adds tourism attraction to the region. The geographic position of Urmia is close to Cenozoic stress fields and faults east of Lake Urmia. In the past 10 years, Urmia has been shaken by several earthquakes—each time with higher magnitude and intensity. Attributed to those incidents, the Iranian Code of Practice for Seismic Resistant Design of Buildings (2800) recently added Urmia to the list of cities with a high risk of earthquake. Given the high rate of population growth and urban development, and the fact that earthquake is a recurring threat to the city, a comprehensive seismic study is necessary for the city.

Description of the Field and Laboratory Experiments

In this work, two field and two laboratory tests were conducted to gather important parameters for training the *NNs*. Standard Penetration Tests (*SPT*) [30] were performed on 71 boreholes distributed throughout the city of Urmia. Fig 3(a) shows the *SPT* equipment setup during in-situ testing. In each borehole, sampling was performed at 2 m intervals up to a depth of 10 m (i.e., 5 samples per borehole). The measured blow counts (SPT-*N or N*) were standardized for 60% energy transfer from the safety hammer to the drill rod. On the soil samples retrieved for laboratory examination, Atterberg limit tests [31] and sieve analyses [32] were performed.

(a) (b) (c) (d)

Fig. 3 - (a) SPT test setup (b) borehole isolation using a concrete block (c) dropping geophones into the borehole (d) Generating waves at ground surface with a hammer

The second field test that was performed was the downhole test [33]. In this test, the stiffness of a soil is determined directly by analyzing the shear and compression waves throughout the length of a borehole (Figs 3(a & b)). Shear waves generated on the ground surface by an external source are received by a sensor that can be moved freely in the borehole. Fig 3(d) shows the process of generating shear waves using a hammer. The traveling time of the seismic waves is analyzed, and seismic velocity of the soil is obtained. Measurements can be done above or below the water table. In order to perform the downhole test, the borehole is dug up to engineering bedrock. The engineering bedrock is defined as the layer in which the underlying stratum has from 300 to 700 m/sec of the shear wave velocity. In this study, the value of 700 m/sec has been assumed as an indicator for engineering bedrock. The depth of the boreholes varied between 10 to 50 m. Wall stabilization of the boreholes was done with PVC pipes of 3 to 6 inches in diameter. The most significant problem during the downhole test was noise caused by nearby construction and traffic load that affected the amplitude and wavelength of the pure shear waves that were originally

produced by the experimental source. This problem was solved by conducting the experiments at night and during the day at times of minimal construction activity inside the city and by integrating statistical correction measures with the testing instrument.

From field and laboratory experiments, the data collection activity resulted in 355 data sets from the 71 boreholes. Fig. 4(a) shows the relative location of the study area. The geographic coordinates and satellite view of Urmia city are also indicated in Figure 4(b). Fig. 4(c) shows borehole locations. The data collected from the *SPT* and downhole tests were used to train the *NNs* in the input and output layers.

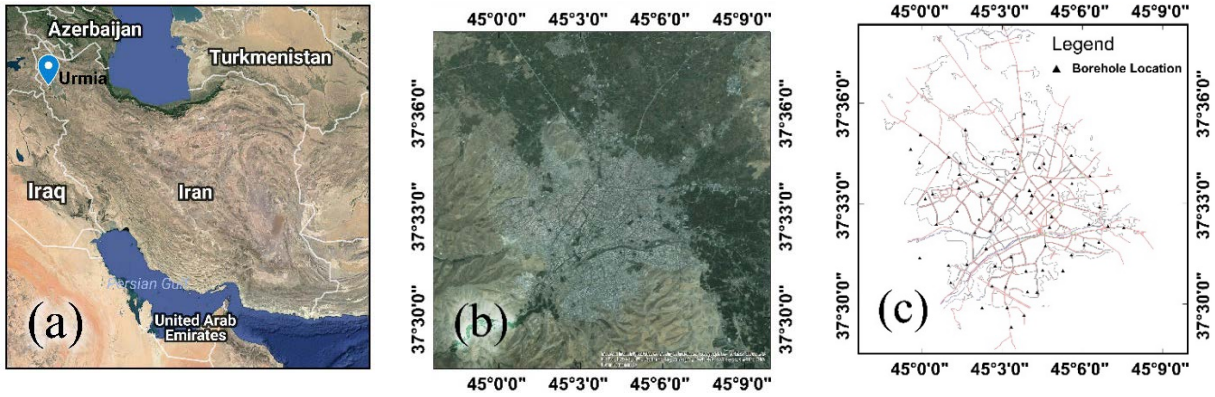

Fig. 4 – (a) the relative location of the study (b) Satellite view of Urmia city; and (c) Location of boreholes.

Results and discussion

Microzonation for shear wave velocity

Practical importance of shear wave velocity, Vs

The importance of shear wave velocity (V_s) in earthquake analyses can be inferred from its strong correlation with the small-strain shear modulus (G_{max}) of a soil. For different strain levels, the shear modulus of a soil will attain different magnitudes. As the shear strain increases, the shear modulus of a soil decreases, as shown in Fig. 5. Such curves are commonly referred to as modulus reduction curves and are used to describe the reduction of the secant modulus with increase in cyclic shear strain. For very small strains (i.e.

less than 10^{-3}), the variation in shear modulus becomes negligible, and it is assumed that the shear modulus remains constant at a value of G_{max}.

From Fig. 5, it can be inferred that accurate information regarding the G_{max} of a given soil is vital in estimating the shear modulus at different strain levels. G_{max} and V_s are two of the most employed parameters in dynamic analysis. These two parameters are employed in soil classification, liquefaction potential, and soil-structure interaction analyses [34]. Given the unit mass (density) and V_s of a certain soil, G_{max} can be estimated using the following equation:

$$G_{\max} = \rho V_s^2 \tag{10}$$

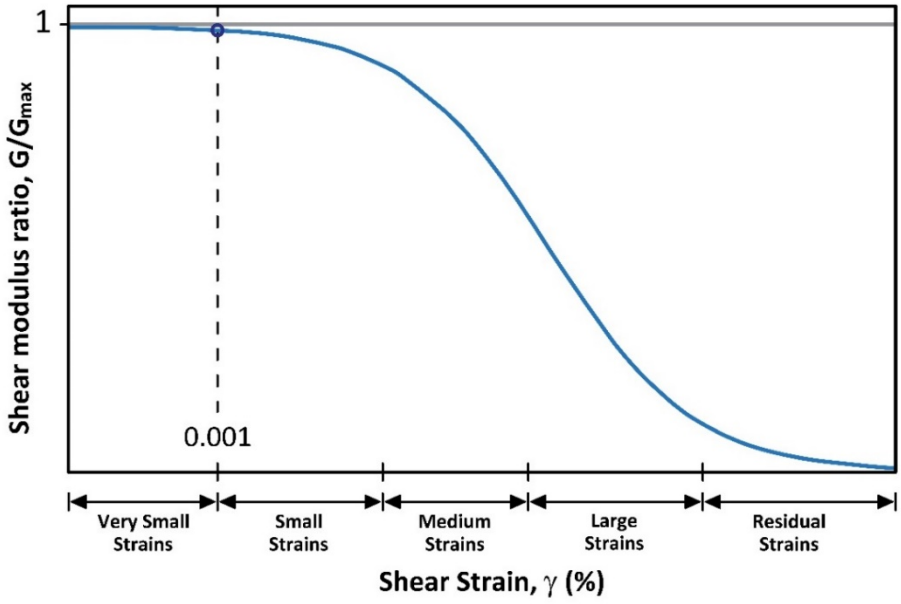

Fig. 5 - Modulus reduction curve

Shear wave velocity determination methods

The shear wave velocity of soils can be obtained from: (1) laboratory measurements; (2) geophysical seismic field measurements; or (3) other indirect measurements. Low strain laboratory tests such as resonant column and bender element tests on undisturbed soil samples are the common laboratory methods used to obtain V_s. Cyclic triaxial apparatus combined with exact measurement of axial strains has also been used for this purpose. Collecting undisturbed

samples is always a challenge because the weak bonds between soil particles start to break during the process of sampling. This in turn degrades the stiffness of samples and dramatically affects the results of small strain laboratory tests. Generally, undisturbed soil sampling on coarse material is impossible unless expensive freezing methods are used [35].

Soil shear wave velocity can also be measured using geophysical methods such as crosshole (CHT), downhole (DHT), seismic cone penetration tests (SCPTs), Micro-tremor, wave propagation analysis at several stations (MASW), and spectral analysis of surface waves (SASW). Since these field experiments are performed at small strain levels, the results of these experiments can be used to estimate G_{max}. Compared to the laboratory methods, the advantage of field measurements is that they naturally cause less disturbance on soil. However, various limitations related to space, cost, and noise, hinder their utilization.

Both laboratory and field measurements are expensive and time consuming and, in many projects, may not be feasible. Thus, the recent trend has shifted towards determining V_s using indirect methods. Indirect methods try to obtain a correlation between V_s and simply acquired geotechnical parameters.

Significant effort has recently been made by researchers to obtain a unique relationship between the shear wave velocity of a soil and other geotechnical parameters. The goal of coming up with these relationships is to cut the cost of obtaining V_s with expensive laboratory and/or field-tests by correlating it to simple geotechnical parameters. Most of the experimental studies focused on directly correlating V_s to *SPT* blow count (N). The most common functional form for the relations proposed in the literature is $V_s = A.N^B$, where the constants A and B are determined by statistical regression of a data set [1]. Some common empirical relationships proposed to relate V_s with N are summarized in Table 1.

Table 1 - Empirical relationships used to estimate V_s from SPT number (N)

References	Soil type		
	All soils	**Sand**	**Clay**
Imai and Yoshimura [36]	$V_s=91N^{0.337}$	$V_s=80.6N^{0.331}$	$V_s=102N^{0.292}$
Seed and Idriss [37]	$V_s=61.4N^{0.5}$	-	-
Seed, Idriss and Arango [38]	-	$V_s=56.4N^{0.5}$	-
Jinan [39]	$V_s=116.1(N+.318)^{0.202}$	-	-
Iyisan [40]	$V_s=51.5N^{0.516}$	-	-
Hasancebi and Ulusay [41]	$V_s=90N^{0.309}$	$V_s=90.82N^{0.319}$	$V_s=97.89N^{0.269}$
Dikmen [42]	$V_s=58N^{0.39}$	$V_s=73N^{0.33}$	$V_s=44N^{0.48}$

Fig. 6 shows the graphical representation of the correlations presented in Table 1 with experimental data from a field study in Urmia. Observing the data scatter, it is clear from Fig. 6 that the SPT number (N) is not sufficient to obtain the shear wave velocity of the soil. Brandenberg, Bellana and Shantz [43] presented an equation to estimate V_s for soils under Caltrans bridges. They gathered data sets from 79 logs over 21 bridges and expressed the natural logarithm of V_s as a function of N and overburden effective stress for sandy, silty, and clayey soils.

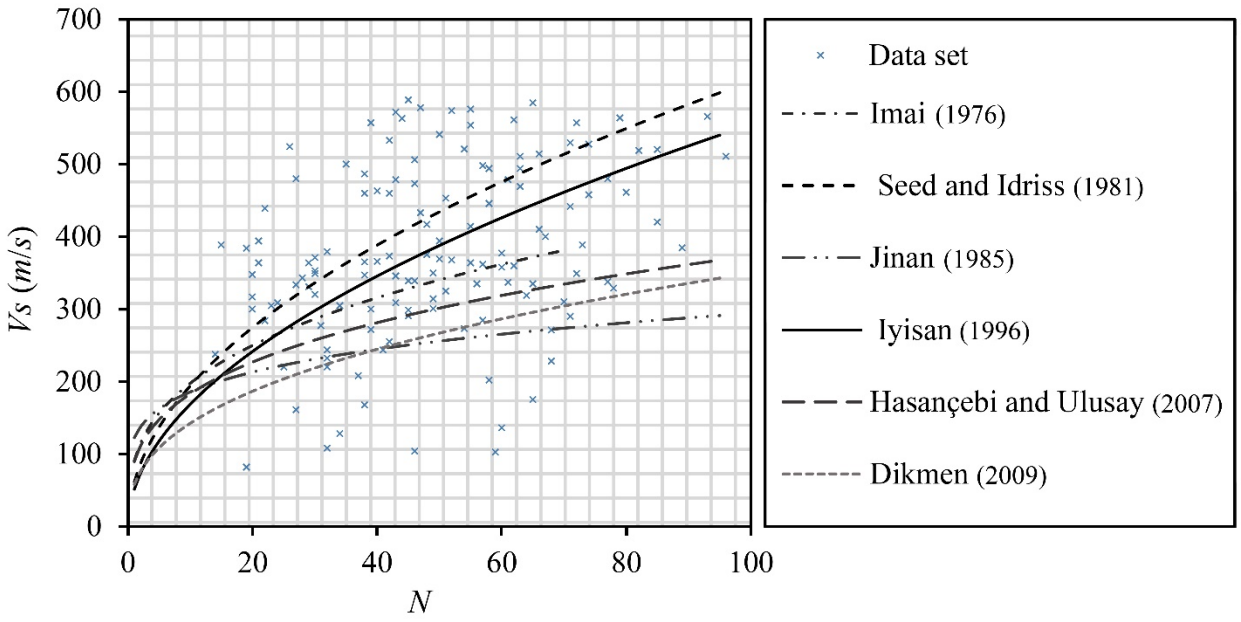

Fig. 6 - Comparison between field data and *N*-based empirical equations (See Table 1) for V_s

The percentage of fines, the depth, and the tip resistance in the cone penetration test are among the other parameters investigated to find a reliable correlation. In addition to overburden stress, the effect of porosity on G_{max} has been investigated by several studies [43-48]. The results revealed that overburden stress and porosity influence the magnitude of G_{max}. Geological age also has an important influence on G_{max}. Pre-consolidation of the soil, on the other hand, has been found to have a little effect on G_{max} [44, 46, 49-55]. There is still an ongoing discussion over the effects of the plasticity index (*PI*) on G_{max}. Some studies show a direct relationship between G_{max} and *PI* [44, 53, 54]. Others reported a reverse relationship [46, 52, 56]. Hardin and Drnevich [53] showed that G_{max} and V_s are dependent on unit weight, porosity, and vertical effective stress, whereas soil type, age, and cementation were shown to impose negligible effect. On the other hand, Dobry and Vucetic [57] showed that with an increase in vertical effective

stress, age, cementation, and pre-consolidation, V_s also increases. They also found out that a reverse relationship governs the correlation between V_s and porosity.

NNs as an indirect method of determining shear wave velocity

In this study, *NNs* were utilized for estimating the shear wave velocity of soils. The input variables were the corrected SPT number (N_{60}), effective overburden pressure (σ'), fines content (F_c), and plasticity index (*PI*). Correlations obtained from *NNs* were integrated with *GIS* by means of a Python script.

As was stated in previous sections of this paper, *SPT* tests were conducted over vertical intervals of 2 m up to a depth of 10 m below the ground surface. This resulted in 5 geographical layers for the soil profile. In each borehole, a downhole test was conducted to obtain shear wave velocity for each 2 m increment. Atterberg limit tests and sieve analysis were performed on samples collected during the *SPT* tests. A total of 355 data points, from 71 boreholes dispersed throughout Urmia, were generated. Table 2 summarizes some of the statistical indices for the data sets. The collected data and associated statistical indices were used for V_s estimation.

Table 2 – Statistical indices for data obtained from field tests

Variables	**Statistics**			
	Max	**Min**	**Mean**	**Standard deviation**
N60	130	4.67	73.82	38.25
σv′(kPa)	176.4	17.3	87.85	49.13
Fc	98	6	71.51	26.6
PI	55.8	0	5.87	9.86
Vs (m/s)	652	90	383.3	123.91

It has been observed that the shear wave velocity changes with a change in overburden pressure. With an increase in soil confinement, the overburden effective stress increases, and the stiffer the soil, the higher the shear wave velocity. The average velocity to any depth H_o, $\overline{V_s}(H_o)$ could be found from available shear wave velocities of the layers. For k layers, $\overline{V_s}(H_o)$ can be expressed as:

$$\overline{V_s}(H_o) = \frac{\sum_{n=1}^{k} H_n \times V_s(H_n)}{H_o} \tag{11}$$

where H_n is the depth measured from the ground surface to the k^{th} layer. In this work, as mentioned before, data was collected at 2 m intervals up to the depth of 10 m. Therefore, in Equation (11), $n = 5$ & $H_o = 10\ m$ will be substituted to calculate $\overline{V_s}(10)$.

The average velocity to 30 m depth, $\overline{V_s}(30)$, is widely used for classifying sites and predicting their response to earthquakes. $\overline{V_s}(30)$ is computed by dividing a distance of 30 m by the travel time from the surface to 30 m. This value is usually used in microzonation to predict the potential of sites to amplify seismic shaking. In most practical cases, samples are not collected for depths greater than 30 m. In addition, ordinary SPT tests are carried out for depths less than or equal to 10 m below the ground. All SPT tests, from field studies in Urmia, were performed to obtain N values for depths not exceeding 10 m. Accordingly, adoption of a statistical means was necessary in calculating $\overline{V_s}(30)$ from $\overline{V_s}(10)$. Boore [58] proposed four methods of extrapolation that can be used to predict $\overline{V_s}(30)$ from available data. One of the methods performs extrapolation using the correlation between $\overline{V_s}(30)$ and $\overline{V_s}(H_o)$ as given in Equation 12, where $\overline{V_s}(H_o)$ represents the value of shear wave velocity for a point located at any depth H_o below the ground.

$$\log \overline{V_s}(30) = a + b \log \overline{V_s}\left(H_o\right) \quad ((12)$$

In the Equation, *a* and *b* are extrapolation coefficients that are constant over the depth H_o. The values of *a* and *b* at $H_o = 10m$ are equal to 0.042 and 1.029, respectively [58].

N_{60}, σ'_v, F_c, and *PI*, and $\overline{V_s}(30)$ are introduced to *NNs* in the training step. Fig. 7 shows the designed *NNs* used to find a correlation between the input variables and $\overline{V_s}(30)$. Table 3 shows the parameters used in the *NNs* for training and testing sets.

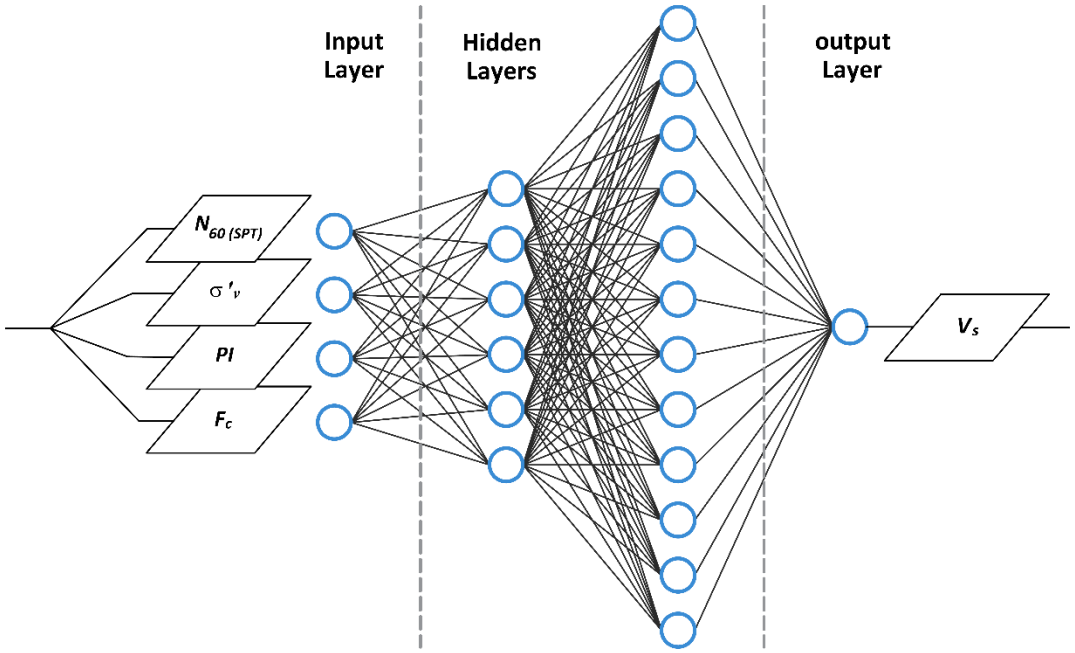

Fig. 7 - Structured *NNs* used to find a correlation between the input variables and $\overline{V_s}(30)$

Table 3 - Values of evaluation parameters and properties of the *NNs* designed for $\overline{V_s}(30)$ estimation

$\overline{V_s}(30)$	R	*MAE*	*RMSE*	Number of hidden layers	Number of neurons on				Activation Function
					IL	HL1	HL2	OL	
Train	0.95	30.29	39.44	2	4	6	12	1	tansig
Test	0.93	33.73	44.19	-	-	-	-	-	-

The values of *MAE* & *RMSE* for training and test steps indicate how well *NNs* perform in estimating $\overline{V_s}(30)$. For example, the results obtained in this work for *RMSE* (i.e., 39.4374 and 44.1928) are indicative of a good performance of the training and testing steps. The trained *NNs* are linked to *GIS* by using Python scripts, and the values of $\overline{V_s}(30)$ are obtained as a continuous spatial information over the entire domain of the site. The *NNs-GIS* interaction is designed in such a way that the resolution of the details will be dynamically improved as additional data is introduced to the *GIS* layers. Fig. 8 shows the microzonation map obtained for $\overline{V_s}(30)$, following the algorithm presented before.

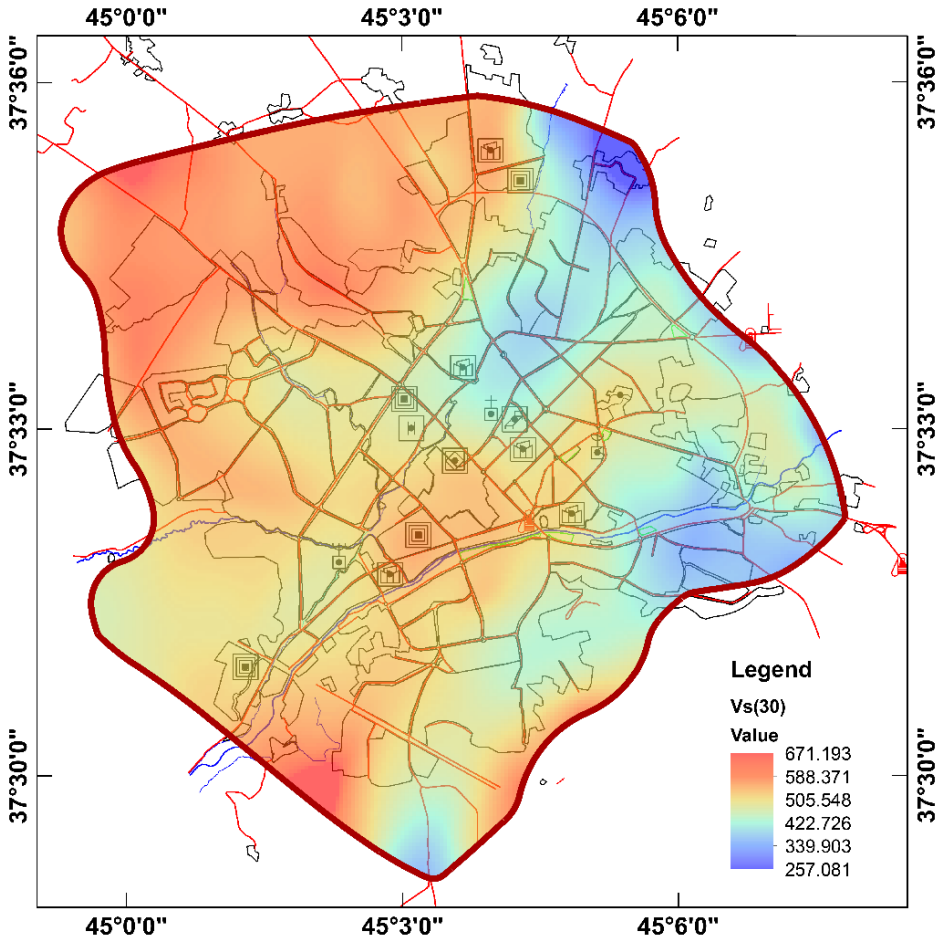

Fig. 8 - Microzonation of Urmia for $\overline{V_s}(30)$

Microzonation for USCS soil classification

Soil classification is a systematic method of grouping soils of similar behavior, describing them, and classifying them. Classification is necessary in the sense that engineers, who deal with the state of practice pertinent to the different soil types across the globe, receive the same information regarding each soil group. Soil classification systems provides the platform upon which helpful details that follow the interpretation of laboratory tests and field observations can systematically be added to each soil group. One of the most common soil classification methods is the Unified Soil Classification System (*USCS*).

Over the engineering field of practice around the world, a number of soil classification systems exist [59-61]. The *USCS* [60] is one of the most widely used classification systems; it groups soils into three major classes and further subdivides each to subclasses based on a specified criteria. *USCS* distinguishes sands from gravels by grain size and further classifies some as "well-graded" and the rest as "poorly-graded". Fig. 9 shows a simplified flowchart, from *USCS*, which can be followed when classifying coarse grained soils. A similar flowchart exists for fine grained soils as well.

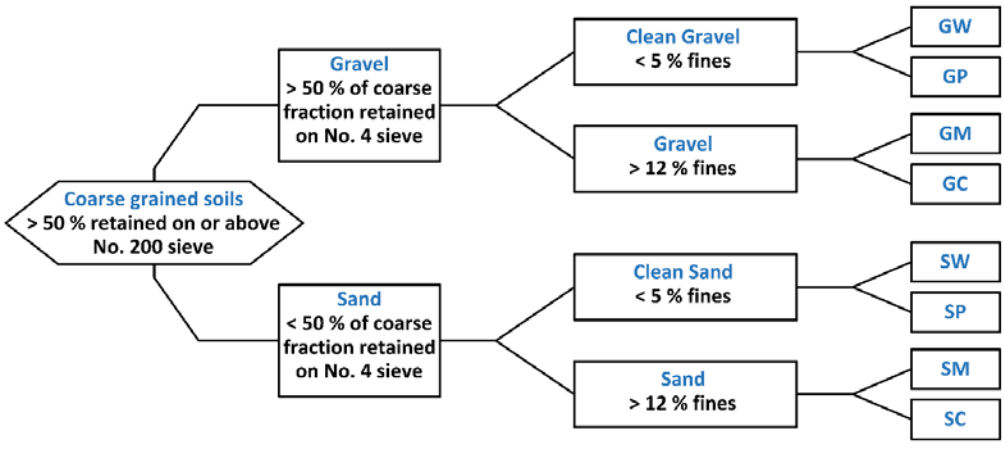

Fig. 9 - *USCS* soil classification approach for coarse-grained soils

Fine grained soils (i.e. silts and clays) are further classified into "high-" or "low-plasticity" by conducting Atterberg limit tests. Fig. 10 shows the "Plasticity Chart" that was first introduced by the work of Arthur Casagrande [62]. Figs. 9 and 10 illustrate the important input variables in the *USCS* system. Closer observation of the inputs in *USCS* could lead to the conclusion that four major parameters are sufficient to be used as input variables for *NNs*. In light of this observation, it can be said that the plastic limit (*PL*), liquid limit (*LL*), and the percentage soil grains that passed Number-200 (F_{200}) and Number-4 (F_4) sieves are the most influential parameters.

In the data used for soil classification in this study, the above four important parameters were determined from laboratory tests. The statistical indices for these parameters are summarized in Table 4.

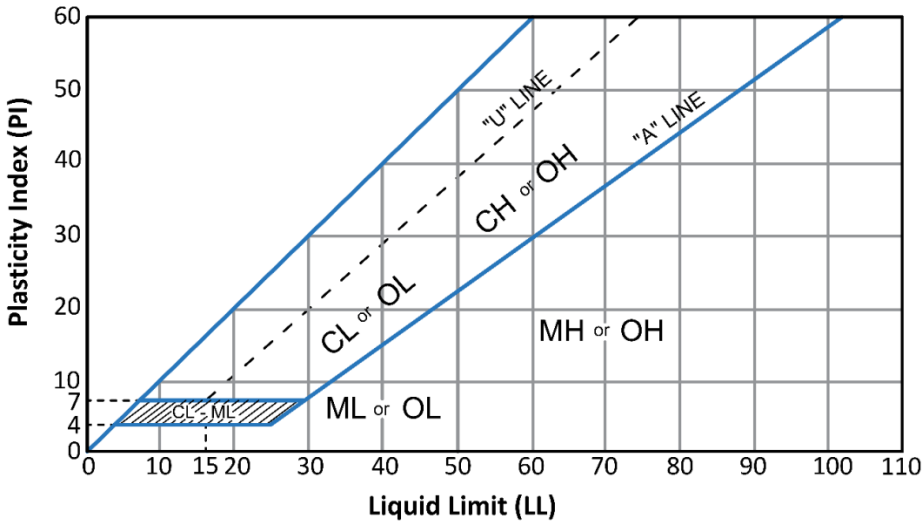

Fig. 10 - *USCS* soil classification approach for fine grained soils

PL, *LL*, F_{200}, F_4, and the *USCS* soil classification obtained after analyzing data from each log are introduced to *NNs* to accomplish the training. Five classes of soils were identified by analyzing field collected samples and collecting information regarding the *PL*, *LL*, F_{200}, and F_{40}. A numeric value was assigned to each of these five classes to enable smooth interpolation between soil

types. Table 5 shows the assigned numbers for each class and their associated names as per the *USCS*.

Table 4 –Statistical indices, obtained from lab tests, used for soil classification

Variables	**Statistics**			
	Max	**Min**	**Mean**	**Standard deviation**
F_4	100	24	87.17	17.32
F_{200}	98	5	68.57	27.61
LL	83	0	10.19	17.35
PL	65.8	0	4.56	7.4

Table 5 – Numeric values assigned for the six soil classes

Assigned numeric value	1	2	3	4	5
Soil class in *USCS*	CL	CL-ML	ML	SM	GM

Fig. 11 shows that the *NNs* developed to find a correlation between the input variables and soil classes. Table 6 presents the parameters used in the *NNs* for training and testing sets.

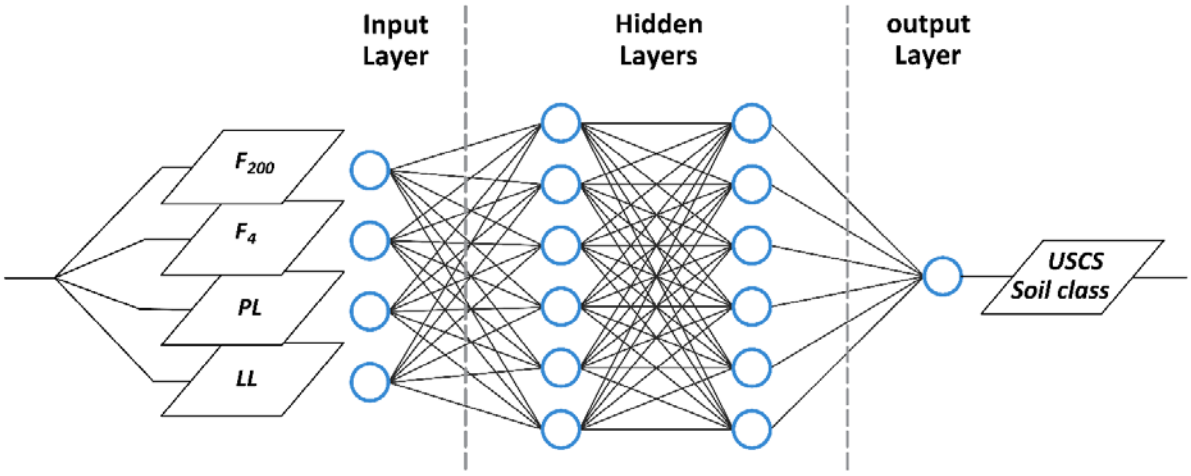

Fig. 113 - Structured *NNs* used to find a correlation between the input variables and soil class

Table 6 – Evaluation parameters and properties of the *NNs* designed for soil classification

Soil class	R	MAE	RMSE	Number of hidden layers	Number of neurons on				Activation Function
					IL	HL1	HL2	OL	
Train	0.99	0.01	0.09	2	4	6	6	1	tansig
Test	0.98	0.02	0.21	-	-	-	-	-	-

The value of RMSE for training and testing steps indicates an excellent performance of *NNs* in estimating soil class in the *USCS* classification system. The same approach is followed to estimate soil class for the entire site. Since the numeric value designation for soil classes (consecutive numbering in this work) plays a vital role, the obtained microzonation might be slightly different if different intervals are assigned between the classes. In cases where irregular intervals are to be used, a weighted scaling of results may be necessary. Fig. 12 shows the *USCS* classification map for the top 2 m layer of Urmia which is obtained by the algorithm introduced in this paper. The exact same algorithm and procedure could be applied to do soil microzonation of the remaining 4 layers (i.e., up to a total depth of 10 m). The results for all of the 5 layers

could be overlapped and used to draw soil profiles at any specific location. The *NNs*-generated soil classification and the microzonation map are found to be in good agreement with the results obtained by performing laboratory and field tests.

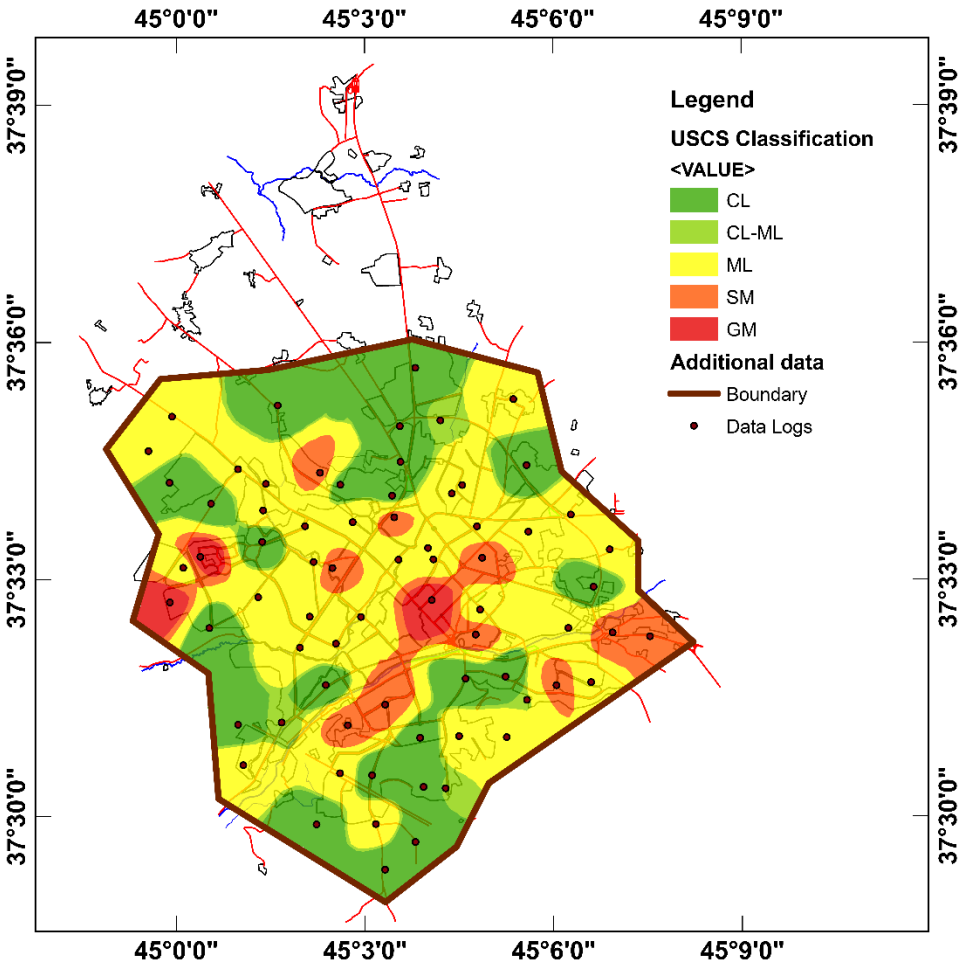

Fig. 12– Microzonation of Urmia for soil classification

Conclusions

An "intelligent" algorithm, that integrated *NNs* and *GIS* was developed and used to produce microzonation maps for shear wave velocity and soil classification. This novel system was designed in a way that microzonation maps are dynamically refined and updated as new data was added to the database. In the proposed algorithm, geographical data layers were checked for null

data points and data lags were estimated using interpolation. The spatial information was extracted, and the complete database was imported to *NNs* for training. The trained *NNs* were embedded to the GIS platform by using Python scripts to carry out the microzonation. The successful application of the proposed algorithm was illustrated using two examples: microzonation of shear wave velocity and soil classification. The performance of the dynamic algorithm was checked with the mean absolute error (*MAE*) and the root mean squared error (*RMSE*). The values of the obtained *MAE* and *RMSE* were indicative of good performance by the integrated *NNs-GIS* system. The approach applied in this paper could be adopted for microzonation of liquefaction potential, landslide risks, settlements, etc. The detailed soil condition maps generated with the proposed algorithm could be used in construction site selection, risk analysis, and geotechnical engineering designs.

References

[1] N. Bellana, Shear Wave Velocity as Function of SPT Penetration Resistance and Vertical Effective Stress at California Bridge Sites, in: Civil and Environmental Engineering, University of California, Los Angeles, 2009, pp. 67.

[2] D. Fäh, E. Rüttener, T. Noack, P. Kruspan, Microzonation of the city of Basel, Journal of Seismology, 1 (1997) 87-102.

[3] R. Tuladhar, F. Yamazaki, P. Warnitchai, J. Saita, Seismic microzonation of the greater Bangkok area using microtremor observations, Earthquake Engineering and Structural Dynamics, 33 (2004) 211-255.

[4] P. Anbazhagan, T. Sitharam, Site characterization and site response studies using shear wave velocity, J. Seismol. Earthquake Eng. , 10 (2008) 53-67.

[5] K.S. Vipin, T.G. Sitharam, P. Anbazhagan, Probabilistic evaluation of seismic soil liquefaction potential based on SPT data, Natural Hazards, 53 (2010) 547-560.

[6] B.R. Cox, J. Bachhuber, E. Rathje, C.M. Wood, R. Dulberg, A. Kottke, R.A. Green, S.M. Olson, Shear wave velocity- and geology-based seismic microzonation of port-au-prince, Haiti, Earthquake Spectra, 27 (2011) 67-92.

[7] H. Murvosh, B. Luke, C. Calderón-Macías, Shallow-to-Deep Shear Wave Velocity Profiling by Surface Waves in Complex Ground for Enhanced Seismic Microzonation of Las Vegas, Nevada, Soil Dynamics and Earthquake Engineering, 44 (2013) 168-182.

[8] A.V. Kalinina, S.M. Ammosov, The study of velocity characteristics of soils according to the MASW method for solving seismic microzonation problems, Voprosy Inzhenernoi Seismologii, 41 (2014) 67–77.

[9] M.J. Garcia-Rodriguez, J.A. Malpica, Assessment of earthquake-triggered landslide susceptibility in El Salvador based on an artificial neural network model, Nat Hazards Earth Syst Sci, 10 (2010) 1307–1315.

[10] D. Kawabata, J. Bandibas, Landslide susceptibility mapping using geological data, a DEM from ASTER images and an artificial neural network (ANN), Geomorphology, 113 (2009) 97-109.

[11] J.D. Paola, R.A. Schowengerdt, A review and analysis of backpropagation neural networks for classification of remotely sensed multi-spectral imager, Int J Remote Sens, 16 (1995) 3033-3058.

[12] S. Lee, J.H. Ryu, K. Min, J.S. Won, Landslide susceptibility analysis using GIS and artificial neural network, Earth Surface Processes & Landforms, 27 (2003) 1361- 1376.

[13] F. Farnood Ahmadi, N. Farsad Layegh, Integration of artificial neural network and geographical information system for intelligent assessment of land suitability for the cultivation of a selected crop, Neural Computing and Applications, 26 (2015) 1311-1320.

[14] X. Li, A.G. Yeh, Neural-network-based cellular automata for simulating multiple land use changes using GIS, International Journal of Geographical Information Science, 16 (2002) 323-343.

[15] B.C. Pijanowski, D.G. Brown, B.A. Shellito, Using neural networks and GIS to forecast land use changes: a land transformation model, Comput Environ Urban Syst 26 (2002) 553-575.

[16] B. Pradhan, S. Lee, Utilization of optical remote sensing data and GIS tools for regional landslide hazard analysis by using an artificial neural network model, Earth Science Frontier, 14 (2007) 143-152.

[17] C. Yoo, J.M. Kim, Tunneling performance prediction using an integrated GIS and neural network, Computers and Geotechnics 34 (2007) 19-30.

[18] B. Pradhan, S. Lee, M.F. Buchroithner, Use of geospatial data for the development of fuzzy algebraic operators to landslide hazard mapping: a case study in Malaysia, Applied Geomatics, 1 (2009) 3-15.

[19] C.I. Ho, M.D. Lin, S.L. Lo, Use of a GIS-based hybrid artificial neural network to prioritize the order of pipe replacement in a water distribution network, Environ. Monit. Assess., 166 (2010) 177-189.

[20] C.R. Chen, H.S. Ramaswamy, M. Marcotte, Neural Network Applications In Heat And Mass Transfer Operations In Food Processing, in: Heat Transfer in Food Processing, WIT Transactions on State-of-the-art in Science and Engineering, 2007, pp. 39-59.

[21] R.P. Lippmann, An introduction to computing with neural nets, ASSP Magazine, IEEE, 4 (1987) 4-22.

[22] K.N. Manahiloh, M. Motalleb Nejad, M.S. Momeni, Optimization of design parameters and cost of geosynthetic-reinforced earth walls using harmony search algorithm, International Journal of Geosynthetics and Ground Engineering, 1 (2015) 1-12.

[23] M. Motalleb Nejad, K.N. Manahiloh, A Modified Harmony Search Algorithm for the Optimum Design of Earth Walls Reinforced with Non-uniform Geosynthetic Layers, International Journal of Geosynthetics and Ground Engineering, 1 (2015) 1-15.

[24] M.T. Hagan, M. Menhaj, Training feed-forward networks with the Marquardt algorithm, IEEE Transaction on Neural Networks, 5 (1999) 989-993.

[25] D.E. Rumelhart, G.E. Hinton, R.J. Williams, Learning representations by back-propagating errors, Nature, 323 (1986) 533-536.

[26] M.T. Hagan, H.B. Demuth, M.H. Beal, Neural Network Design, PWS Publishing Company, Boston, 1996.

[27] MATLAB, The Language of Technical Computing (R2016a), in, Math Works Inc, 2016.

[28] S. Rajasekaran, G.A. Vijayalakshmi Pai, Neural networks, fuzzy logic and genetic algorithm: synthesis and applications (with cd), PHI Learning Pvt. Ltd., 2003.

[29] N.A.C. Cressie, Statistics for Spatial Data, John Wiley & Sons, Inc., 2015.

[30] ASTM Standard D1586, Standard Test Method for Standard Penetration Test (SPT) and Split-Barrel Sampling of Soils, in, ASTM International, West Conshohocken, 2011.

[31] ASTM Standard D4318, Standard test methods for liquid limit, plastic limit, and plasticity index of soils, in, ASTM International, West Conshohocken, 2010.

[32] ASTM Standard C136/C136M, Standard Test Method for Sieve Analysis of Fine and Coarse Aggregates, in, ASTM International, West Conshohocken, 2014.

[33] ASTM Standard D7400, Standard Test Methods for Downhole Seismic Testing, in, ASTM International, West Conshohocken, 2014.

[34] Y. Choi, J.P. Stewart, Nonlinear site amplification as function of 30 m shear wave velocity, Earthq spectra, 21 (2005) 1-30.

[35] A. Ghorbani, Y. Jafarian, M.S. Maghsoudi, Estimating shear wave velocity of soil deposits using polynomial neural networks: Application to liquefaction, Comput Geosci, 44 (2012) 86-94.

[36] T. Imai, M. Yoshimura, The relation of mechanical properties of soils to P and S wave velocities for soil ground in Japan, in, Urana Research Institute, OYO Corporation, Japan, 1976.

[37] H.B. Seed, I.M. Idriss, Evaluation of liquefaction potential sand deposits based on observation of performance in previous earthquakes, in: ASCE National Convention, Missouri, 1981.

[38] H.B. Seed, I.M. Idriss, I. Arango, Evaluation of liquefaction potential using field performance data, J Geotech Eng, 109 (1983) 458-482.

[39] Z. Jinan, Correlation between seismic wave velocity and the number of blow of SPT and Depths, Chin J Geotech Eng (ASCE), (1987) 92-100.

[40] R. Iyisan, Correlations between shear wave velocity and in-situ penetration test results, Technical journal of Turkish Chamber of Civil Engineers, 7 (1996) 371-374.

[41] N. Hasancebi, R. Ulusay, Empirical correlations between shear wave velocity and penetration resistance for ground shaking assessments, Bull Eng Geol Environ, 66 (2007) 203-213.

[42] Ü. Dikmen, Statistical correlations of shear wave velocity and penetration resistance for soils, J Geophys Eng, 6 (2009) 61-72.

[43] S. Brandenberg, N. Bellana, T. Shantz, Shear wave velocity as a statistical function of standard penetration test resistance and vertical effective stress at Caltrans bridge sites, Soil Dynamics and Earthquake Engineering, 30 (2010) 1026-1035.

[44] T. Kim, M. Novak, Dynamic properties of some cohesive soils of Ontario, Canadian Geotechnical Journal, 18 (1981) 371-389.

[45] M. Jamiolkowski, S. Leroueil, D.C.F. Lo Presti, Design parameters from theory to practice, in: Geo-Coast Yokohama, Japan, 1991, pp. 877-917.

[46] T. Kagawa, Moduli and damping factors of soft marine clays, Journal of Geotechnical Engineering. ASCE, 118 (1992) 1360-1375.

[47] S. Teachavorasinskun, P. Thongchim, P. Lukkunappasit, Shear modulus and damping of soft Bangkok clays, Canadian Geotechnical Journal, 39 (2002) 1201-1208.

[48] G. Lanzo, A. Pagliaroli, P. Tommasi, F.L. Chiocci, Simple shear testing of sensitive, very soft offshore clay for wide strain range, Canadian Geotechnical Journal, 46 (2009) 1277 - 1288.

[49] S. Afifi, F. Richart, Stress-history effects on shear modulus of soils, Japanese Society of Soil Mechanics and Foundations, 13 (1973) 77-95.

[50] D.G. Anderson, K.H. Stokoe II, Shear Modulus: A Time-Dependent Soil Property: Dynamic Geotechnical Testing. , ASTM STP 654, (1978) 66 - 90.

[51] M.B. Darendeli, Development of a new family of normalized modulus reduction and material damping curves, in, University of Texas at Austin, Austin, Texas, 2001.

[52] P. Kallioglou, T. Tika, K. Pitilakis, Shear Modulus and Damping Ratio of Cohesive Soils, Journal of Earthquake Engineering, 12 (2008) 879-913.

[53] B.O. Hardin, V.P. Drnevich, Shear modulus and damping in soils: measurement and parameter effects (terzaghi leture), J Soil Mech Found Div, 98 (1972) 603-624.

[54] M. Vucetic, R. Dobry, Effect of soil plasticity on cyclic response, Journal of Geotechnical Engineering, 117 (1991) 89-107.

[55] S. Rampello, G. Viggiani, Panel discussion: The dependence of G_o on stress state and history in cohesive soils, in: Shibuya, Mitachi, Miura (Eds.) Prefailure Deformation of Geomaterials, Balkema, Rotterdam, 1995, pp. 1155 – 1160.

[56] S. Yamada, M. Hyodo, R. Orense, S.V. Dinesh, Initial shear modulus of remolded sand-clay mixtures, Journal of Geotechnical and Geoenvironmental Engineering, 134 (2008) 960-971.

[57] R. Dobry, M. Vucetic, Dynamic properties and seismic response of soft clay deposits, Department of Civil Engineering, Rensselaer Polytechnic Institute, 1988.

[58] D.M. Boore, Estimating Vs(30) (or NEHRP Site Classes) from Shallow Velocity Models (Depths < 30 m) Bulletin of the Seismological Society of America, 94 (2004) 591-597.

[59] AASHTO, AASHTO Materials, in: Part 1 Specifications, ASTM, Washington, D.C., 1982.

[60] ASTM Standard D2487, Standard Practice for Classification of Soils for Engineering Purposes (Unified Soil Classification System), in, ASTM International, West Conshohocken, 2011.

[61] USDA, Soil Taxonomy, in: A basic system of soil classification for making and interpreting soil surveys, U.S. Government printing office, Washington, D.C., 1999.

[62] A. Casagrande, Classification and Identificatino of soils, Transactions, ASCE, 113 (1948) 901-930.